

Chiral Rashba spin textures in ultra-cold Fermi gases

Jay D. Sau¹, Rajdeep Sensarma¹, Stephen Powell¹, I. B. Spielman^{1,2}, and S. Das Sarma¹

¹*Condensed Matter Theory Center and Joint Quantum Institute, Department of Physics, University of Maryland, College Park, Maryland 20742-4111, USA*

²*National Institute of Standards and Technology, Gaithersburg, Maryland, 20899.*

Spin-orbit coupling is an important ingredient in many recently discovered phenomena such as the spin-Hall effect and topological insulators. Of particular interest is topological superconductivity, with its potential application in topological quantum computation. The absence of disorder in ultra-cold atomic systems makes them ideal for quantum computation applications, however, the spin-orbit (SO) coupling schemes proposed thus far are experimentally impractical owing to large spontaneous emission rates in the alkali fermions. In this paper, we develop a scheme to generate Rashba SO coupling with a low spontaneous emission extension to a recent experiment. We show that this scheme generates a Fermi surface spin texture for ⁴⁰K atoms, which is observable in time-of-flight measurements. The chiral spin texture, together with conventional *s*-wave interactions leads to topological superconductivity and non-Abelian Majorana quasiparticles.

PACS numbers: 67.85.Lm, 03.65.Vf, 03.67.Lx

Introduction: The physics of coupled spin and motional degrees of freedom, and associated phenomena such as the spin-Hall effect [1, 2], are a subject of intense interest: first in semiconductors [3] and now in cold-atom systems [4–6]. Recent predictions of new topological states of matter based on spin-orbit (SO) coupling such as topological insulators [7] and topological superconductors [8] have generated great excitement both experimentally and theoretically. In solids, SO coupling occurs naturally in systems with broken inversion symmetry, while SO coupling must be engineered for cold atoms, where laser fields break inversion symmetry.

Time-reversal (TR) symmetry breaking topological superconductor [8–10] are one particularly interesting class of systems that may be realized in the presence of SO coupling. These support Majorana quasiparticle excitations which obey non-Abelian statistics [11]. Systems exhibiting non-Abelian statistics have topologically degenerate ground states that can potentially be used for topological quantum computation [12, 13]. The promise of realizing the elusive Majorana particles together with the topological ground state degeneracy in superconducting systems [14] has inspired considerable experimental effort studying superconductivity in SO coupled solid state systems in magnetic fields [15, 16].

To understand the role of SO coupling in topological superfluidity [17], consider a system of fermionic atoms in a Zeeman field $V_Z > E_F, k_B T$, with attractive *s*-wave interactions [Fig. 1(a)]. Pairing is in the spin-singlet channel, i.e., with opposite spins. Here T is the temperature, and $E_F = \hbar^2 k_F^2 / 2M$ is the Fermi energy of atoms with mass M and Fermi momentum $\hbar k_F$. Since $V_Z > E_F$, the fermions are completely spin polarized and the resulting state is an ideal non-interacting Fermi gas. On the other hand, in the presence of Rashba SO coupling [$H_R = \alpha(\sigma_x p_y - \sigma_y p_x)$] with strength α , where $\sigma_{x,y,z}$ are Pauli matrices, the spins at the Fermi-surface are

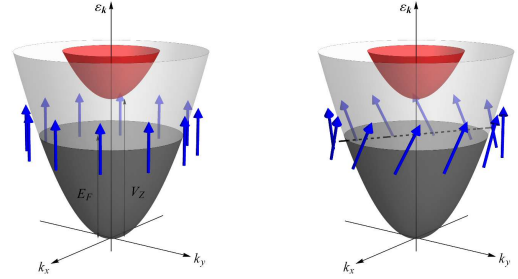


FIG. 1: (a) Uniform Fermi surface spin texture in a system of fermions with Zeeman splitting V_Z . The Fermi surface is taken to be in the lower band (spin polarized-up) with Fermi energy E_F . (b) Chiral Fermi surface spin texture in a system of fermions with Zeeman coupling V_Z and Rashba SO coupling. The Rashba SO coupling causes a counter-clockwise canting of spins (canted arrows) on the otherwise spin-up Fermi surface. The canting-induced overlap between time-reversed spins at opposite points \vec{k} and $-\vec{k}$ on the Fermi surface allows fermion pairing by a microscopic *s*-wave interaction leading to *p*-wave topological superfluidity.

canted [Fig. 1(b)]. Since pairs of fermions at momenta $\hbar\vec{k}$ and $-\hbar\vec{k}$ on the Fermi surface have a component in the singlet-channel [10, 17], an attractive *s*-wave interaction with coupling constant g generates an effective *p*-wave interaction $\tilde{g} \sim g\alpha k_F / V_Z$ at the Fermi surface. This interaction leads to pairing and a superfluid quasiparticle gap. Such a completely gapped superfluid state occupying a single Fermi surface has been shown to be topological with zero-energy Majorana modes as low-energy excitations of the system [9]. Thus SO coupling together with Zeeman splitting would lead to topological superconductivity with Majorana fermions. Unlike topological phases such as topological insulators, topological superfluids are created by arbitrarily weak SO coupling [9]. The strength

of SO coupling determines the size of the gap and thus the robustness of the topological phase.

The three ingredients needed to realize TR breaking topological superconductors are: ordinary s -wave interactions, Zeeman splitting, and SO coupling [9, 10]. The first two ingredients are already well-established in cold atomic systems. Several schemes for realizing SO coupling in cold atomic systems [4–6], where state-dependent laser fields lead to effective SO-coupled Hamiltonians for the laser-dressed atoms, are the basis of proposals for topological systems such as topological insulators [18] and topological superconductors [17, 19]. Despite the theoretical interest in such SO coupling schemes, they have thus far eluded experiment. One reason for this is that the simpler schemes such as the tripod-scheme [4] require resonant coupling to achieve the required SO coupling, and spontaneous emission from nearby excited states in actual experimental systems becomes prohibitive.

An exciting recent development is the first experimental realization of a restricted class of SO coupled Hamiltonians in a bosonic cold atomic system [20, 21]. This experiment used the three levels in the ^{87}Rb $F = 1$ ground state manifold, and reduces spontaneous emission by working in the far-detuned limit [21, 22]. In addition, by using the lowest energy manifold of dressed states collisional decay was eliminated [23]. The resulting SO coupling, [24] $H_{R+D} \propto \sigma_y p_x$ can in principle lead to a superfluid gap. Unfortunately, for fermions this equal sum of Rashba and Dresselhaus SO coupling results in a non-topological gapless p_x -superfluid.

Here, we design a cold-atom system with Rashba SO coupling using an extension of the existing setup used to realize H_{R+D} . The SO coupling here is a function of the intensity of the applied lasers, while, in previous schemes, the SO coupling is geometric and independent of laser strength for large enough coupling [4]. Although all Raman coupling schemes are susceptible to spontaneous emission, our scheme uses small two-photon coupling, minimizing spontaneous emission. Atom-chip based systems, where spatially varying magnetic fields replace Raman couplings, have recently been proposed to realize systems such as topological insulators that require strong SO coupling [24].

Following the description of our proposed experimental setup, we verify analytically that the effective Hamiltonian in the weak Raman coupling limit has the requisite Rashba SO coupling form. Going beyond this limit, we show by direct numerical calculation that the eigenstates have the chiral momentum-space spin texture required to create p -wave interactions with no nodes. Varying the relative laser intensities allows us to tune the SO coupling between the H_R (Rashba) and H_{R+D} forms [3]. The spin texture calculation predicts the results of time-of-flight measurements of spin-density, which would directly establish that the necessary effective Hamiltonian to cre-

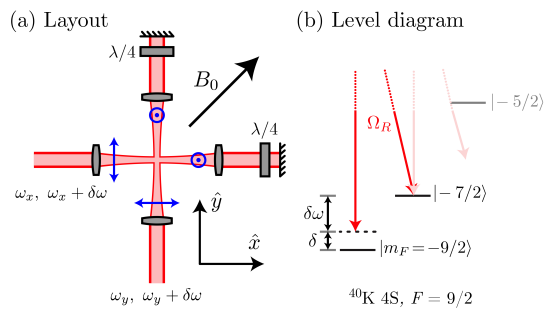


FIG. 2: (a) Laser fields applied to an ultra-cold ^{40}K gas generate a Rashba SO coupling between the $m_F = -7/2$ and $m_F = -9/2$ states. Effective Zeeman couplings that vary along \hat{x} and \hat{y} directions are generated by Raman-coupling these states through an excited state e by lasers of frequencies $\omega_x, \omega_x + \delta\omega$ along \hat{x} and $\omega_y, \omega_y + \delta\omega$ along \hat{y} . Appropriately tuning the phases of these lasers at the atomic gas generates Rashba and Dresselhaus SO coupling. (b) Atomic level structure (solid lines) of an effective spin-1/2 atom with hyperfine states $|\sigma_z = +1\rangle \equiv |m_F = -7/2\rangle$ and $|\sigma_z = -1\rangle \equiv |m_F = -9/2\rangle$. The detuning δ from the state $|\sigma_z = +1\rangle$ sets the position independent Zeeman coupling along σ_z .

ate the Majorana particle has been created in the atomic Fermi gas (all one needs to do is to add the s -wave superfluidity through the appropriate Feshbach resonance.).

Setup: We propose to illuminate a sample of quantum degenerate fermionic ^{40}K in its electronic ground state with two pairs of counterpropagating “Raman” lasers. These beams are far-detuned about $\Delta \sim 2$ THz to the red of the $4S_{1/2}$ to $4P_{1/2}$ (D1) transition (~ 400 THz), and each beam is composed of two frequencies $\omega_{x,y}$ and $\omega_{x,y} + \delta\omega$ which drive transitions between different sub-levels of the ground state $F = 9/2$ hyperfine manifold. As pictured in Fig. 2, a magnetic field $B_0 \approx 200$ G along $\hat{x} + \hat{y}$ resolves the different Zeeman sub-levels, and owing to a sizable quadratic Zeeman shift only one pair of states is Raman-resonant, here $|m_F = -9/2\rangle$ and $|m_F = -7/2\rangle$. We will refer to these states as pseudo-spin $|\sigma_z = -1\rangle$ and $|\sigma_z = +1\rangle$ respectively. The excited states $4P_{1/2}$ and $4P_{3/2}$ through which the Raman coupling between $|\sigma_z = \pm 1\rangle$ is driven will be collectively referred to as e .

Effective Zeeman coupling: The two pairs of lasers in our setup along \hat{x} and \hat{y} respectively, are detuned from the excited state e by slightly different detunings Δ_x and Δ_y , so that they induce independent Raman couplings. The Rabi coupling between states $|\sigma_z = \pm 1\rangle$ and the excited state e , driven by the pair of lasers along $a = x$ or y together with their reflected counterparts, can be written as a complex two-component spinor amplitude $\mathbf{f}_{\sigma_z}^{(a)}(\vec{r})$. The spinor potential $\mathbf{f}^{(a)}(\vec{r}) = \Gamma^{(a)}[\mathbf{f}_{\sigma_z=+1}^{(a,+)} e^{i\vec{G}^{(a)} \cdot \vec{r}} + \mathbf{f}_{\sigma_z=-1}^{(a,-)} e^{-i\vec{G}^{(a)} \cdot \vec{r}}]$ results from lasers traveling in opposite directions; the spinors $\mathbf{f}^{(a,\pm)}$ encode the relative phases of the lasers along $\pm \hat{a}$ and at

frequencies ω_a and $\omega_a + \delta\omega$. Here $\Gamma^{(a)}$ is the overall coupling constant along \hat{a} .

In the far-detuned limit, where all energy eigenvalues of states of interest are much smaller than the detuning Δ_a , each pair of lasers generates an effective spatially dependent Zeeman potential within the rotating wave approximation (RWA), given by

$$\mathbf{F}^{(a)}(\vec{r}) = \mathbf{f}^{(a)}(\vec{r})\mathbf{f}^{(a)\dagger}(\vec{r})/\Delta_a. \quad (1)$$

To generate Rashba and Dresselhaus SO coupling we choose $\mathbf{f}^{(x,\pm)}$ to be eigenvectors of σ_y (i.e., $\sigma_y \mathbf{f}^{(x,\pm)} = \pm \mathbf{f}^{(x,\pm)}$) and $\mathbf{f}^{(y,\pm)}$ to be eigenvectors of σ_x (i.e., $\sigma_x \mathbf{f}^{(y,\pm)} = \mp \mathbf{f}^{(y,\pm)}$). With this choice the effective Zeeman potential $\mathbf{F}(\vec{r}) = \sum_a \mathbf{F}^{(a)}(\vec{r})$ is

$$\begin{aligned} \mathbf{F}(\vec{r}) &= \Omega_R^{(y)} \sin(G_0 y) \sigma_y - \Omega_R^{(x)} \sin(G_0 x) \sigma_x \\ &+ \left[\Omega_R^{(x)} \cos(G_0 x) + \Omega_R^{(y)} - \cos(G_0 y) \right] \sigma_z \end{aligned} \quad (2)$$

where $\Omega_R^{(a)} = \Gamma^{(a)2}/\Delta^{(a)}$ is the effective Raman coupling in the direction a . Here we have taken $\vec{G}^{(x)} = G_0 \hat{x}/2$ and $\vec{G}^{(y)} = G_0 \hat{y}/2$ where $G_0 = (2\omega_a + \delta\omega)/c = 4\pi/\lambda$ and $\lambda \sim 0.7 \mu\text{m}$ is the wavelength of light [26]. In Eqn. 2, we ignored a constant and irrelevant spin-independent shift. From the above equations, we find that only the relative phases of the beams propagating in the same direction (with the same a) contribute to the effective Zeeman coupling. Furthermore, the only effect of changing the relative phase of counterpropagating lasers (e.g $+\hat{x}$ and $-\hat{x}$) is to shift the origin of the system.

Bloch Hamiltonian: Since the effective position dependent Zeeman potential $\mathbf{F}(\vec{r})$ is periodic in space, the Hamiltonian for our system has a discrete translational symmetry. Using Bloch's theorem, the spinor eigenstate of the Hamiltonian of the system can be expanded as $\phi_{\vec{k}}^{(n)}(\vec{r}) = \sum_{\vec{G}} \mathbf{C}_{\vec{k}+\vec{G}}^{(n)} e^{i(\vec{k}+\vec{G})\cdot\vec{r}}$ such that the eigenstate $\phi_{\vec{k}}^{(n)}$ has a conserved wavevector \vec{k} defined modulo reciprocal lattice vectors $\vec{G} = n_1 \vec{G}^{(x)} + n_2 \vec{G}^{(y)}$. The Bloch eigenvectors $\phi_{\vec{k}}^{(n)}$ at wavevector \vec{k} are eigenvectors of the Bloch Hamiltonian at momentum $\hbar\vec{k}$

$$\mathbf{H}_{\vec{k}}(\vec{k}+\vec{G}; \vec{k}+\vec{G}') = \left(\frac{\hbar^2 |\vec{k} + \vec{G}|^2}{2M} \mathbf{1} + \frac{\delta}{2} \sigma_z \right) \delta_{\vec{G}, \vec{G}'} + \mathbf{F}(\vec{G} - \vec{G}') \quad (3)$$

where $\mathbf{F}(\vec{G})$ is the Fourier transform of the laser-induced spatially varying Zeeman coupling $\mathbf{F}(\vec{r})$. Here δ is the detuning induced Zeeman splitting obtained by choosing the detuning of the respective lasers as shown in Fig. 2(b). For \vec{k} restricted to the first Brillouin zone (FBZ), the set of Bloch eigenvectors $\phi_{\vec{k}}^{(n)}$, labeled by band-index n , and corresponding energy eigenvalues $\epsilon_{\vec{k}}^{(n)}$ can be determined using $\mathbf{H}_{\vec{k}} \phi_{\vec{k}}^{(n)} = \epsilon_{\vec{k}}^{(n)} \phi_{\vec{k}}^{(n)}$.

Small Ω_R limit: The explicit Rashba-Dresselhaus form of the effective Hamiltonian for the two lowest bands (which serve as a pseudo-spin basis) can be derived in the limit of large recoil energy $E_R = \frac{\hbar^2}{2M\lambda^2} \approx h \times 8.4 \text{ kHz} \gg \delta, \Omega_R$ for $\lambda \approx 770 \text{ nm}$. Absent Raman coupling ($\Omega_R = 0$), the Hamiltonian $\mathbf{H}_{\vec{k}}$ is diagonal in the spin and reciprocal lattice-vector (\vec{G}) basis. In this case, for wavevectors \vec{k} in the FBZ, the lowest pair of bands contain only states with $\vec{G} = 0$, while the higher bands, separated in energy by at least E_R , contain states with $\vec{G} \neq 0$.

A small Raman coupling $\Omega_R \ll E_R$ couples the unperturbed ($\Omega_R = 0$) system such that the Schrödinger equation is written as:

$$[k^2 \mathbf{1} + \frac{\delta}{2} \sigma_z - \epsilon_{\vec{k}}^{(n)} \mathbf{1}] \mathbf{C}_{\vec{k}}^{(n)} + \sum_{\vec{G} \neq 0} \mathbf{F}(-\vec{G}) \mathbf{C}_{\vec{k}+\vec{G}}^{(n)} = 0 \quad (4)$$

$$[|\vec{k} + \beta \vec{G}_\gamma|^2 - \epsilon_{\vec{k}}^{(n)}] \mathbf{C}_{\vec{k}+\vec{G}}^{(n)} + \mathbf{F}(\vec{G}) \mathbf{C}_{\vec{k}}^{(n)} = 0, \quad (5)$$

where we have set $\hbar^2/2M = 1$, and have ignored the contribution of $\vec{G} \neq 0$ to the second term in Eq. 5 which is of order $(\Omega_R/E_R)^3$. Furthermore, we ignored the contribution $\mathbf{F}(\vec{G} = 0)$ to the equation, which leads to an overall energy shift. The unperturbed states in the higher bands, with a small contribution, can be adiabatically eliminated by substituting $\mathbf{C}_{\vec{k}+\vec{G}}^{(n)}$ from Eq. 5 into Eq. 4; we obtain the effective Schrödinger equation

$$\left[(k^2 - \epsilon_{\vec{k}}^{(n)}) \mathbf{1} + \frac{\delta}{2} \sigma_z - \sum_{\vec{G} \neq 0} \frac{\mathbf{F}(-\vec{G}) \mathbf{F}(\vec{G})}{|\vec{k} + \vec{G}|^2 - \epsilon_{\vec{k}}^{(n)}} \right] \phi_{\vec{k}} = 0. \quad (6)$$

For $\epsilon_{\vec{k}}^{(n)} \ll E_R$, the $\epsilon_{\vec{k}}^{(n)}$ dependence of the last term is negligible.

The effective Schrödinger equation (Eq. 5) for the lowest pair of bands in the FBZ takes the familiar Rashba form

$$\left[(k^2 - \mu - \epsilon_{\vec{k}}^{(n)}) \mathbf{1} + \frac{\delta}{2} \sigma_z + \frac{\Omega_R^2}{2E_R G_0} (k_y \sigma_x - k_x \sigma_y) \right] \phi_{\vec{k}}^{(n)} = 0, \quad (7)$$

when $\Omega_R^{(x)} = \Omega_R^{(y)} = \Omega_R$. Pure Dresselhaus coupling is obtained by interchanging the spinors $\mathbf{f}^{(x,\pm)}$, while varying the ratio of $\Omega_R^{(x)}/\Omega_R^{(y)}$ tunes SO coupling from the pure Rashba type to the $R + D$ type.

Numerical solution: We verified the Rashba coupling obtained from the perturbative calculation by numerically diagonalizing the Hamiltonian (Eq. 3). As is clear from the representative band structure shown in Fig. 3(a), there is a non-degenerate band at the lowest energy. For these parameters, a reasonably high density Fermi gas ($n \sim 1.2\lambda^{-2}$), at a temperature of $k_B T = E_F/8 \approx 0.04 E_R$, would be in the single Fermi surface limit with a Fermi energy of $E_F \approx 0.32 E_R$. The

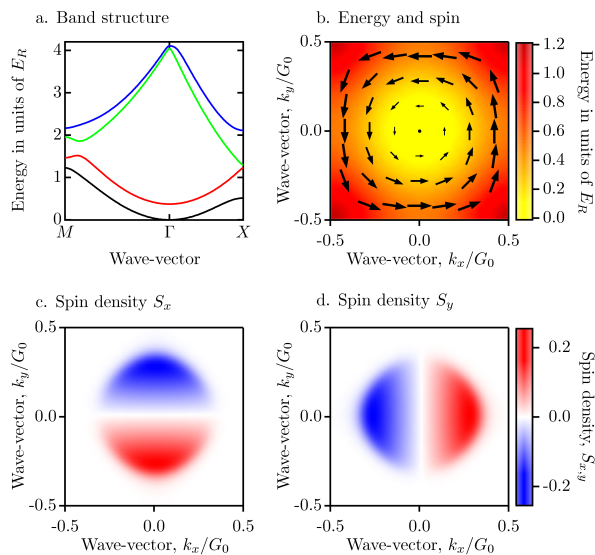


FIG. 3: (a) Band structure for the proposed system for the parameters $\Omega_R = \Gamma^2/\Delta = 0.8E_R$ together with $\delta = 0.4E_R$. For ^{40}K , the recoil energy $E_R = h \times 8.4$ kHz. The points $\vec{k} = (k_x, k_y) = (0.5, 0.5)G_0, (0, 0)$ and $(0.5, 0)G_0$ have been labelled M, Γ and X on the horizontal-axis respectively. For these parameters, the lowest energy-band is non-degenerate and isotropic. (b) Dispersion and spin texture in the lowest band, showing nearly circular constant-energy contours for small wavevectors (color scale) and chiral spin texture characteristic of Rashba SO coupling (arrows indicate x - y spin components). (c) Momentum $S_x(\vec{k})$ spin density. The corresponding time-of-flight phase-contrast measurement of S_x spin density should show a p_y symmetry. (d) Momentum $S_y(\vec{k})$ spin density. The corresponding time-of-flight phase-contrast measurement of S_y spin density should show a p_x symmetry.

spin texture in the occupied band, shown in Fig. 3(b-d), is calculated from the spin-expectation value

$$\vec{s}(\vec{k}) = \sum_{\vec{G}} \mathbf{C}_{0\vec{k}+\vec{G}}^\dagger \vec{\sigma} \mathbf{C}_{0\vec{k}+\vec{G}} \quad (8)$$

and is chiral, confirming the Rashba SO coupling.

Time-of-flight phase-contrast detection: Our calculations [Fig. 3(c,d)] show a momentum-dependent chiral spin texture such that the S_x and S_y spin densities have p_y and p_x symmetries in momentum space respectively. The chiral spin texture at the Fermi surface can be detected using phase-contrast imaging [25] following time-of-flight (TOF) expansion, where the final position (reflecting the initial momentum) will be correlated with initial spin. Phase-contrast imaging of the atoms can

measure spin densities along arbitrary directions allowing one to measure S_x and S_y directly.

Conclusion: We proposed a precise, and experimentally feasible, scheme to generate Rashba SO coupling which eliminates the heating problem of the tripod scheme due to spontaneous emission. We show by direct calculations that our proposed scheme should lead to the observation of chiral spin textures using a phase-contrast technique. The spin texture together with conventional s -wave inter-atomic interactions should lead to effective p -wave pairing and hence topological superconductivity and non-Abelian Majorana fermions.

This work was supported by DARPA-QuEST, JQI-NSF-PFC, LPS-NSA and ARO's atomtronics MURI.

-
- [1] S. Murakami, N. Nagaosa, and S.-C. Zhang, *Science* **301**, 1348 (2003).
 - [2] J. Sinova et. al., *Phys. Rev. Lett.* **92**, 126603 (2004).
 - [3] J. D. Koralek et al., *Nature* **458**, 610-613 (2009).
 - [4] J. Ruseckas, G. Juzeliunas, P. Ohberg, M. Fleischhauer, *Phys. Rev. Lett.* **95**, 010404 (2005).
 - [5] S. Zhu et al., *Phys. Rev. Lett.* **97**, 240401 (2006).
 - [6] K. Osterloh, et al., *Phys. Rev. Lett.* **95**, 010403 (2005).
 - [7] M. Z. Hasan and C. L. Kane, *Rev. Mod. Phys.* **82**, 3045 (2010).
 - [8] A. P. Schnyder, S. Ryu, A. Furusaki and A. W. W. Ludwig, *Phys. Rev. B* **78**, 195125 (2008).
 - [9] J. D. Sau, R. M. Lutchyn, S. Tewari, and S. Das Sarma, *Phys. Rev. Lett.* **104**, 040502 (2010).
 - [10] J. D. Sau, et al., *Phys. Rev. B.* **82**, 214509 (2010).
 - [11] F. Wilczek, *Fractional Statistics and Anyon Superconductivity* (World Scientific, Singapore) (1990).
 - [12] A. Kitaev, *Ann. Phys.* **303**, 2 (2003).
 - [13] C. Nayak, et al., *Rev. Mod. Phys.* **80**, 1083 (2008).
 - [14] N. Read and D. Green, *Phys. Rev. B* **61**, 10267 (2000).
 - [15] M. Franz, *Physics* **3**, 24 (2010).
 - [16] F. Wilczek, *Nature Physics* **5**, 614 (2009).
 - [17] C. Zhang, S. Tewari, R. M. Lutchyn, and S. Das Sarma, *Phys. Rev. Lett.* **101**, 160401 (2008).
 - [18] T. D. Stanescu, et al., *Phys. Rev. A* **79**, 053639 (2009); T.D. Stanescu, et al., *Phys. Rev. A* **82**, 013608 (2010).
 - [19] M. Sato, Y. Takahashi, and S. Fujimoto *Phys. Rev. Lett.* **103**, 020401 (2009).
 - [20] Y.-J. Lin, et al., *Phys. Rev. Lett.* **102**, 130401 (2009).
 - [21] Y.-J. Lin, K. Jimenez-Garcia, I. B. Spielman, submitted.
 - [22] J. Higbie, D. M. Stamper-Kurn, *Phys. Rev. Lett.* **88**,090401 (2002).
 - [23] I. B. Spielman et al., *Phys. Rev. A* **73**, 020702 (2006).
 - [24] N. Goldman et. al, arXiv:1002.0219 (2010).
 - [25] M. Vengalattore, et al., *Phys. Rev. Lett.* **98**, 200801 (2007).
 - [26] We have neglected the slightly different magnitudes of the wavevectors $\vec{G}_\beta^{(a)}$ corresponding to ω_a and $\omega_a + \delta\omega$.